Analysis of Alternating Current Electroosmotic Flows in a Rectangular Microchannel

David Erickson and Dongqing Li*

Department of Mechanical and Industrial Engineering, University of Toronto, 5 King's College Road, Toronto, Ontario, Canada, M5S 3G8

Received December 19, 2002. In Final Form: April 17, 2003

Electroosmotic flow is widely used as a primary method of species transport in microfluidic devices. The recent introduction of several alternating current (ac) based microfluidic applications has led to enhanced interest in time periodic electroosmotic flows. In this work, an analytical solution, via a Green's function formulation, is developed for ac electroosmotic flow through a rectangular microchannel for the case of a sinusoidal applied electric field. The response of the flow field to excitation by more complex waveforms is also investigated using numerical simulations. It is shown that the steady time periodic (after the effects of the initial impulse are dissipated) velocity profile is characterized by the ratio of the period of oscillation to the time scale for viscous diffusion, by the surface ζ-potential distribution, and by the channel aspect ratio. Impulsively started flows are also shown to exhibit interesting transient behavior resulting in a net positive velocity at the channel midpoint during the initial cycles prior to reaching the steady state oscillation. The influence of the particular excitation waveform is demonstrated to be more significant at lower frequencies since the bulk flow has more time to respond to instantaneous changes in the applied potential.

I. Introduction

The development of Lab-on-Chip devices involves the incorporation of many of the necessary components and functionality of a typical laboratory on to a small glass or polymer chip. These miniaturized systems are slated to offer significant advantages to analytical chemists as they can, in principle, minimize consumption of reagents (by using smaller sample volumes), lessen analysis times, and reduce operation and manufacturing costs. While species transport on these devices can be accomplished by a number of techniques (for example pressure or thermopneumatically driven flow), the lack of moving parts and the favorable velocity profile have made electrokinetic means such as electroosmosis and electrophoresis the preferred method.

Recently the development of a series of related applications has led to enhanced interest in time periodic electroosmotic flows or alternating current (ac) electroosmosis (i.e., electroosmotic flow induced by unsteady applied electric fields). Oddy, Santiago, and Mikkelsen[1] for example proposed and experimentally demonstrated a series of schemes for enhanced species mixing in microfluidic devices using ac electric fields. In addition, Oddy et al.[1] also presented an analytical flow field model, based on a surface slip condition approach, for an axially applied (i.e., along the flow axis) ac electric field in an infinitely wide microchannel. Comprehensive models for this slit channel geometry have also been presented by Dutta and Beskok,[2] who developed an analytical model for an applied sinusoidal electric field using a nonlinear Poisson−Boltzmann double-layer distribution, and Söderman and Jönsson,[3] who examined the transient flow field caused by a series of different pulse designs.

As an alternative to traditional direct current (dc) electroosmosis, a series of novel techniques have been developed to generate bulk flow using ac fields. For example, Green et al.[4] experimentally observed peak flow velocities on the order of hundreds of micrometers per second near a set of parallel electrodes subject to two ac fields, 180° out of phase with each other. The effect was subsequently modeled using a linear double-layer analysis by Gonzàlez et al.[5] Using a similar principal, both Brown et al.[6] and Studer et al.[7] presented microfluidic devices that incorporated arrays of nonuniformly sized embedded electrodes which, when subject to an ac field, were able to generate a bulk fluid motion. Also using embedded electrodes, Selvaganapathy et al.[8] demonstrated what they termed fr-EOF or bubble-free electroosmotic flow in which a creative periodic waveform was used to yield a net bulk flow while electrolytic bubble formation was theoretically eliminated. Alternating current fields in microfluidic structures have also proven to be promising for dielectrophoretic separation of particles on Lab-on-Chip devices[9] or as a method to enhance electroosmotic flow through ion exchange membranes.[10]

In this study, a combined theoretical and numerical approach is taken to investigate the time periodic electroosmotic flow in a rectangular microchannel. An analytical solution to the velocity field, based on a Green's function formulation, is presented for a linearized Poisson−Boltzmann double-layer model and an applied sinusoidal electric field, while more complex cases (including

* To whom correspondence should be addressed. Fax: (416) 978-7753. E-mail: dli@mie.utoronto.ca.

(1) Oddy, M. H.; Santiago, J. G.; Mikkelsen. J. C. *Anal. Chem.* **2001**, *73*, 5822.
(2) Dutta, P.; Beskok, A. *Anal. Chem.* **2001**, *73*, 5097.
(3) Söderman, O.; Jönsson, B. *J. Chem. Phys.* **1996**, *105*, 10300.
(4) Green, N. G.; Ramos, A.; Gonzàlez, A.; Morgan, H.; Castellanos, A. *Phys. Rev. E.* **2000**, *61*, 4011.
(5) Gonzàlez, A.; Ramos, A.; Green, N. G.; Castellanos, A.; Morgan, H. *Phys. Rev. E* **2000**, *61*, 4019.
(6) Brown, B. D.; Smith, C. G.; Rennie, A. R. *Phys. Rev. E* **2002**, *63*, 016305 1.
(7) Studer, V.; Pépin, A.; Chen, Y.; Ajdari, A. *Microelectron. Eng.* **2002**, *61*−*62*, 915.
(8) Selvaganapathy, P.; Ki, Y.-S. L.; Renaud, P.; Mastrangelo, C. H. *J. Microelectromech. Syst.* **2002**, *11*, 448.
(9) Hughes, M. P. *Electrophoresis* **2002**, *23*, 2569.
(10) Barragán, V. M.; Bauzá, C. R. *J. Colloid Interface Sci.* **2000**, *230*, 359.

10.1021/la027035s CCC: $25.00
Published on Web 05/29/2003

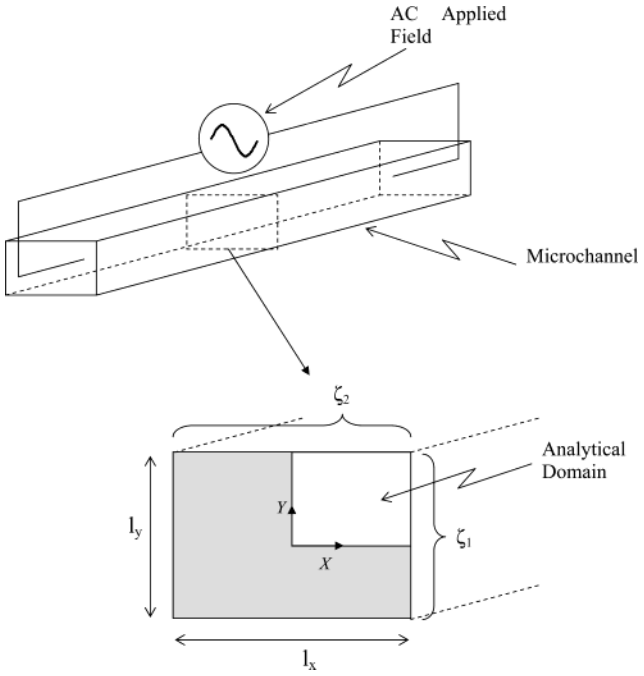

Figure 1. System geometry and analytical domain.

different waveforms) are studied numerically using a finite element technique.[11] The rectangular channel geometry is more representative of that encountered in actual microfluidic systems. The models presented here allow us to investigate the effects of, among other things, system transients due to the initial impulse, nonuniform ζ-potential distribution, and channel aspect ratio on the ac electroosmotic flow field.

II. Analysis of Time Periodic Electroosmotic Flow in a Rectangular Microchannel

As described earlier, in this study the time periodic electroosmotic flow in a straight, rectangular microchannel, as shown in Figure 1, will be examined. For generality, the model will be developed such that the upper and lower surfaces can have a different ζ-potential than the side walls (denoted ζ_1 and ζ_2, respectively). Assuming a fully developed flow field and considering the geometric symmetry, the analytical domain can be reduced to the upper left-hand quadrant of the channel cross section as shown in Figure 1.

When a liquid comes into contact with a solid, the formation of an interfacial charge causes a rearrangement of the local free ions in the liquid so as to produce a thin region of non-zero net charge density, commonly referred to as the electrical double layer (EDL), near the interface. The application of an external electric field results in a net body force on the free ions within the EDL inducing a bulk fluid motion called electroosmotic flow. For pure electroosmotic flows (i.e., absent of any pressure gradients) of incompressible liquids, the Navier−Stokes equations take the following form,[2,12]

$$\rho_f \frac{\partial v}{\partial t} = \mu \nabla^2 v + \rho_e E(\omega t) \tag{1}$$

where v is the flow velocity, t is time, ρ_f is the fluid density, ρ_e is the net charge density, μ is the fluid viscosity, and $E(\omega t)$ is a general time periodic function with a frequency $\omega = 2\pi f$ which describes the applied electric field strength. As was observed experimentally by Oddy et al.[1] at very high applied electric field strengths (greater than 100 V/mm), the flow system may become unstable (chaotic) and thus this should be considered the upper limit on the applicability of eq 1.

II.A. Double-Layer Field. The electric double-layer distribution, ψ, in a rectangular microchannel, required in order to evaluate ρ_e in eq 1, can in its most general form be described by the Poisson equation shown below,

$$\epsilon \nabla^2 \psi = \rho_e \tag{2}$$

where ϵ is the dielectric constant of the fluid medium. In the absence of a significant convective or electrophoretic disturbance to the double layer,[13,14] the net charge density field can be described by a Boltzmann distribution, which takes the form (assuming a symmetric electrolyte)[15]

$$\rho_e = -2zen_0 \sinh\left(\frac{ze\psi}{k_b T}\right) \tag{3}$$

where z is the valence, e is the charge of an electron, n_0 is the bulk electrolyte concentration, k_b is the Boltzmann constant, and T is the temperature. Combining eq 2 and eq 3 and introducing the nondimensional double-layer potential, $\Psi = ze\psi/k_bT$, and nondimensional double-layer thickness $K = D_h\kappa$ (where D_h is the hydraulic diameter of the channel, $D_h = 4l_xl_y/2(l_x + l_y)$, and κ is the Debye−Hückel parameter) yields the nonlinear Poisson−Boltzmann distribution equation,

$$\tilde{\nabla}^2\Psi - K^2 \sinh(\Psi) = 0 \tag{4}$$

where the $\sim$ signifies that the spatial variables in the gradient operator have been nondimensionalized with respect to D_h (i.e., $X = x/D_h$, $Y = y/D_h$). Equation 4 is subject to the symmetry conditions along the channel center axes, $\partial\Psi/\partial X = 0$ at $X = 0$ and $\partial\Psi/\partial Y = 0$ at $Y = 0$, and the appropriate Dirichlet conditions at the channel walls, $\Psi = Z_1$ at $X = L_x/2$ and $\Psi = Z_2$ at $Y = L_y/2$ (where $Z_{1,2} = ze\zeta_{1,2}/k_bT$, $L_x = l_x/D_h$, and $L_y = l_y/D_h$).

For the one-dimensional case, Burgreen and Nakache[16] developed an analytical solution to the nonlinear Poisson−Boltzmann equation for a finite double-layer thickness; however, for multidimensional space and more complex geometries the full form of eq 4 must be solved numerically. In the interest of developing an analytical solution for the situation of interest here, eq 4 will be linearized using the Debye−Hückel approximation,[12,15] yielding

$$\tilde{\nabla}^2\Psi - K^2\Psi = 0 \tag{5}$$

In general, the Debye−Hückel approximation is considered valid when $|ze\zeta| < k_bT$, which in principle limits us to cases where $|\zeta| \leq 25$ mV at room temperature. The actual ramifications of using this approximation at higher ζ-potentials will be explored in greater detail later. For the rectangular geometry shown in Figure 1, an analytical solution to eq 5, subject to the aforementioned boundary

(11) Erickson, D.; Li, D. *Langmuir* **2002**, *18*, 1883.
(12) Yang, C.; Li, D. *Colloids Surf., A* **1998**, *143*, 339.
(13) Erickson, D.; Li, D. *Langmuir* **2002**, *18*, 8949.
(14) Erickson, D.; Li, D. *J. Phys. Chem. B*, submitted.
(15) Hunter, R. J. *Zeta Potential in Colloid Science, Principals and Applications*; Academic Press: New York, 1981.
(16) Burgreen, D.; Nakache, F. R. *J. Phys. Chem.* **1964**, *68*, 1084.

conditions, can be obtained using a separation of variables technique as was done by Yang and Li,[12] yielding

$$\Psi(X,Y) = \sum_{n=1}^{\infty}\frac{4(-1)^{n+1}}{\pi(2n-1)}\left[Z_1\cos(\lambda_n X)\frac{\cosh([\lambda_n{}^2+K^2]^{1/2}Y)}{\cosh([\lambda_n{}^2+K^2]^{1/2}L_Y/2)}\right] + \sum_{n=1}^{\infty}\frac{4(-1)^{n+1}}{\pi(2n-1)}\left[Z_2\cos(\mu_n Y)\frac{\cosh([\mu_n{}^2+K^2]^{1/2}X)}{\cosh([\mu_n{}^2+K^2]^{1/2}L_X/2)}\right] \quad (6)$$

where λ_n and μ_n are the eigenvalues given by $\lambda_n = \pi(2n-1)/L_X$ and $\mu_n = \pi(2n-1)/L_Y$, respectively.

II.B. Flow Field. Introducing the nondimensional time, $\theta = \mu t/\rho_f D_h{}^2$, and the nondimensional frequency, $\Omega = \rho_f D_h{}^2\omega/\mu$, scaling the flow velocity by the electroosmotic slip velocity, $V = vze\mu/\epsilon E_z k_b T$, where E_z is a constant equivalent to the strength of the applied electric field, and combining eq 1 with eq 2 and eq 4 yield the nondimensional flow equation,

$$\frac{\partial V}{\partial \theta} = \tilde{\nabla^2}V - K^2\sinh(\Psi)F(\Omega\theta) \quad (7)$$

where F is a general periodic function of unit magnitude such that $E(\Omega\theta) = E_z F(\Omega\theta)$. Along the channel axes, eq 7 is subject to a symmetry boundary conditions, $\partial V/\partial X = 0$ at $X = 0$ and $\partial V/\partial Y = 0$ at $Y = 0$, while no-slip conditions are applied along the solid channel walls, $V = 0$ at $X = L_x/2$ and $Y = L_y/2$. As before, in the interest of developing an analytical solution to eq 7, the Debye−Hückel approximation is implemented and $F(\Omega\theta)$ is chosen to be a sinusoid function, resulting in the following form of the equation,

$$\frac{\partial V}{\partial \theta} = \tilde{\nabla^2}V - K^2\Psi(X,Y)\sin(\Omega\theta) \quad (8)$$

Using a Green's function formulation, an analytical solution to eq 8, subject to the homogeneous boundary conditions discussed above, can be obtained which takes the form

$$V(X,Y,\theta) = -K^2\int_{\tau=0}^{\theta}d\tau\int_{X'=0}^{L_X}\int_{Y'=0}^{L_Y}\Psi(X',Y')\sin(\Omega\tau)G(X,Y,\theta|X',Y',\tau)\,dX'\,dY' \quad (9)$$

where $G(X,Y,\theta|X',Y',\tau)$ is the Green function. For the finite domain used here, the Green function can be found from the eigenvectors of the homogeneous problem,[12,17] yielding

$$G(X,Y,\theta|X',Y',\tau) = \frac{16}{L_x L_Y}\sum_{l=1}^{\infty}\sum_{m=1}^{\infty}[\exp(-[\lambda_l{}^2+\mu_m{}^2][\theta-\tau])][\cos(\lambda_l X)\cos(\lambda_l X')][\cos(\mu_m Y)\cos(\mu_m Y')] \quad (10)$$

where λ_l and μ_m are the same eigenvalues as those for eq 6. Substituting eq 10 and eq 6 into eq 9 and solving yields

$$V(X,Y,\theta) = \frac{-64K^2}{L_X L_Y}\sum_{l=1}^{\infty}\sum_{m=1}^{\infty}\sum_{n=1}^{\infty}\frac{(-1)^{n+1}}{\pi(2n-1)}\cos(\lambda_l X)\cos(\mu_m Y)\times \left[\frac{(\lambda_l{}^2+\mu_m{}^2)\sin(\Omega\theta)-\Omega\cos(\Omega\theta)+\Omega\exp(-[\lambda_l{}^2+\mu_m{}^2]\theta)}{(\lambda_l{}^2+\mu_m{}^2)^2+\Omega^2}\right][f_{1mn}+f_{2ln}] \quad (11)$$

where f_{1mn} and f_{2ln} are given by

$$f_{1mn} = \begin{cases}0 & n\neq m\\ \dfrac{Z_1\mu_m(-1)^{m+1}}{\lambda_n{}^2+\mu_m{}^2+K^2}\left(\dfrac{L_X}{4}\right) & n=m\end{cases} \quad (12a)$$

$$f_{2ln} = \begin{cases}0 & n\neq l\\ \dfrac{Z_2\lambda_l(-1)^{l+1}}{\mu_n{}^2+\lambda_l{}^2+K^2}\left(\dfrac{L_Y}{4}\right) & n=l\end{cases} \quad (12b)$$

Equation 11 and eqs 12a and 12b represent the full solution to the transient flow problem. The equation can be somewhat simplified in cases where the time periodic solution (i.e., after the influence of the initial conditions has dissipated) is of interest. As these initial effects are represented above by the exponential term in eq 11, the time periodic solution has the form shown below,

$$V(X,Y,\theta) = \frac{-64K^2}{L_X L_Y}\sum_{l=1}^{\infty}\sum_{m=1}^{\infty}\sum_{n=1}^{\infty}\frac{(-1)^{n+1}}{\pi(2n-1)}\cos(\lambda_l X)\cos(\mu_m Y)\left[\frac{(\lambda_l{}^2+\mu_m{}^2)\sin(\Omega\theta)-\Omega\cos(\Omega\theta)}{(\lambda_l{}^2+\mu_m{}^2)^2+\Omega^2}\right][f_{1mn}+f_{2ln}] \quad (13)$$

III. Results and Discussion

In the preceding section, an analytical description of the uniaxial electroosmotic flow in a rectangular microchannel has been developed based on a Green's function formulation. The governing parameter in the above formulation is Ω which represents the ratio of the diffusion time scale ($t_{diff} = \rho_f D_h{}^2/\mu$) to the period of the applied electric field ($t_E = 1/\omega$). Figure 2 compares the time periodic velocity profiles (as computed from eq 13) in the upper left-hand quadrant of a square channel for two cases, (a) $\Omega = 30$ and (b) $\Omega = 625$ (corresponding to frequencies of 500 Hz and 10 kHz in a 100 μm square channel or equivalently a 100 μm and a 450 μm square channel at 500 Hz). To illustrate the essential features of the velocity profile, a relatively large double-layer thickness has been used, $\kappa = 3\times10^6$ m^{-1} (corresponding to a bulk ionic concentration $n_0 = 10^{-6}$ M), and a uniform surface potential of $\zeta = -25$ mV was selected to remain within the bounds imposed by the Debye−Hückel linearization. For a discussion on the effects of double-layer thickness, the reader is referred to Dutta and Beskok.[2] From Figure 2, it is apparent that the application of the electrical body force results in a rapid acceleration of the fluid within the double layer.[1−3] In the case where the diffusion time scale is much greater than the oscillation period (high Ω, Figure 2b), there is insufficient time for fluid momentum to diffuse far into the bulk flow and thus while the fluid within the double layer oscillates rapidly the bulk fluid remains nearly

(17) Beck, J. V.; Cole, K. D.; Haji-Sheikh, A.; Litkouhi, B. *Heat Conduction Using Green's Functions*; Taylor & Francis: London, 1992.

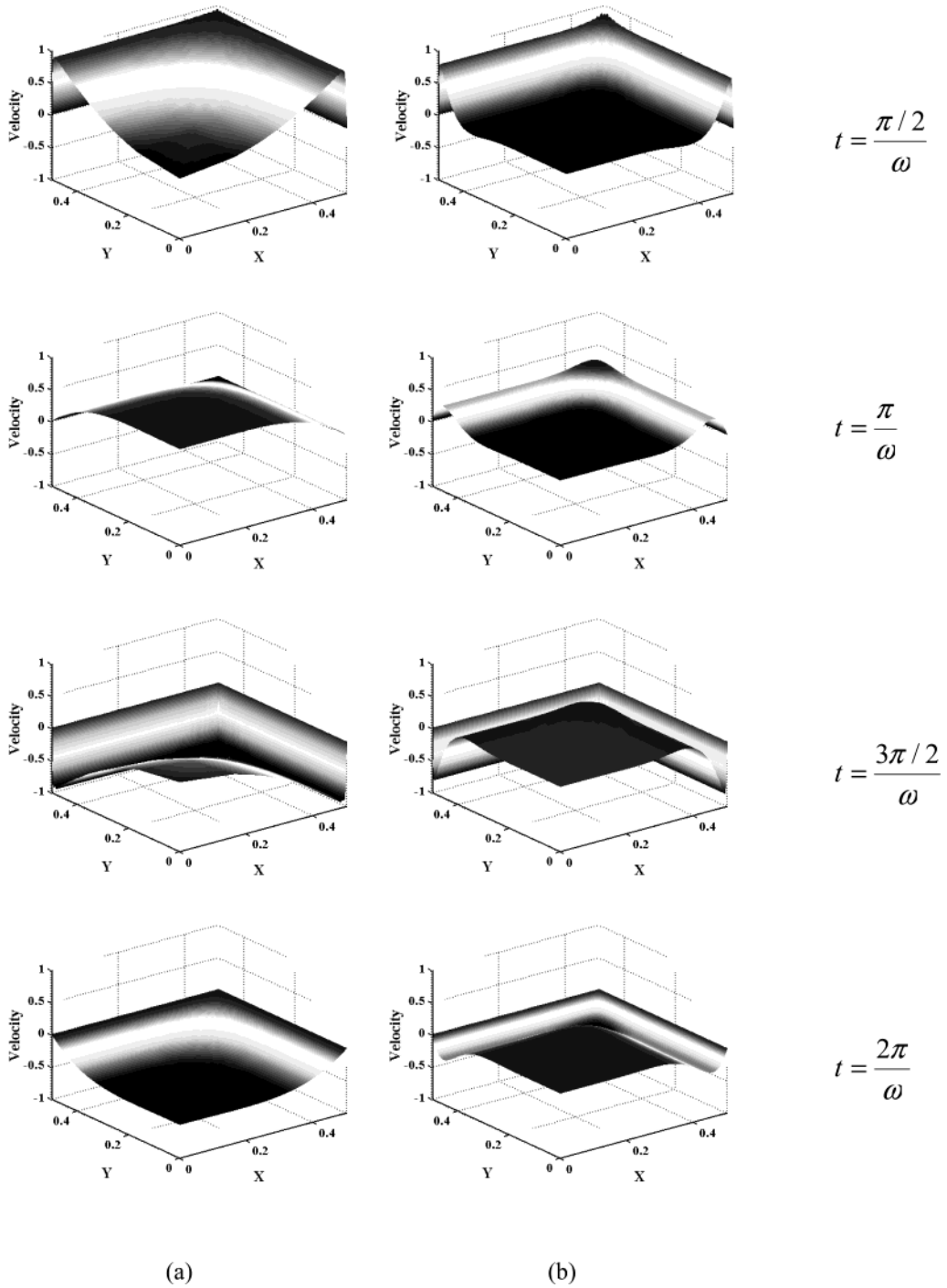

Figure 2. Steady state time periodic electroosmotic velocity profiles in a square microchannel at (a) $\Omega = 30$ and (b) $\Omega = 625$ (equivalent to an applied electric field frequency of (a) 500 Hz and (b) 10 kHz in a 100 μm by 100 μm square channel).

stationary. At $\Omega = 30$, there is more time for momentum diffusion from the double layer; however, the bulk fluid still lags behind the flow in the double layer (this out-of-phase behavior will be discussed shortly). Extrapolating from these results, when $\Omega < 1$, such that momentum diffusion is faster than the period of oscillation, the plug type velocity profile characteristic of steady state electroosmotic flow would be expected at all times.

Another interesting feature of the velocity profiles shown in Figure 2 is the local velocity maximum observed near the corner (most clearly visible in the $\Omega = 625$ case at $t = \pi/2\omega$ and $t = \pi/\omega$). The intersection of the two walls results in a region of double-layer overlap and thus an increased net charge density (mathematically this results from the superposition of both f_{1mn} and f_{2ln} in this region). This peak in the net charge density increases the ratio of the electrical body force to the viscous retardation allowing it to respond more rapidly to changes in the applied electric field and thus resulting in a local maximum in the transient electroosmotic flow velocity.

As was alluded to above, the finite time required for momentum diffusion will inevitably result in some degree of phase shift between the applied electric field and the flow response in the channel. From Figure 2, however, it is apparent that within the limit of $\Omega > 1$, this phase shift is significantly different in the double-layer region than in the bulk flow. Figure 3 ($\Omega = 30$) and Figure 4 ($\Omega = 625$) illustrate this steady state phase shift at two points, (a) the channel midpoint, characteristic of the bulk liquid motion, and (b) the velocity maximum near the channel

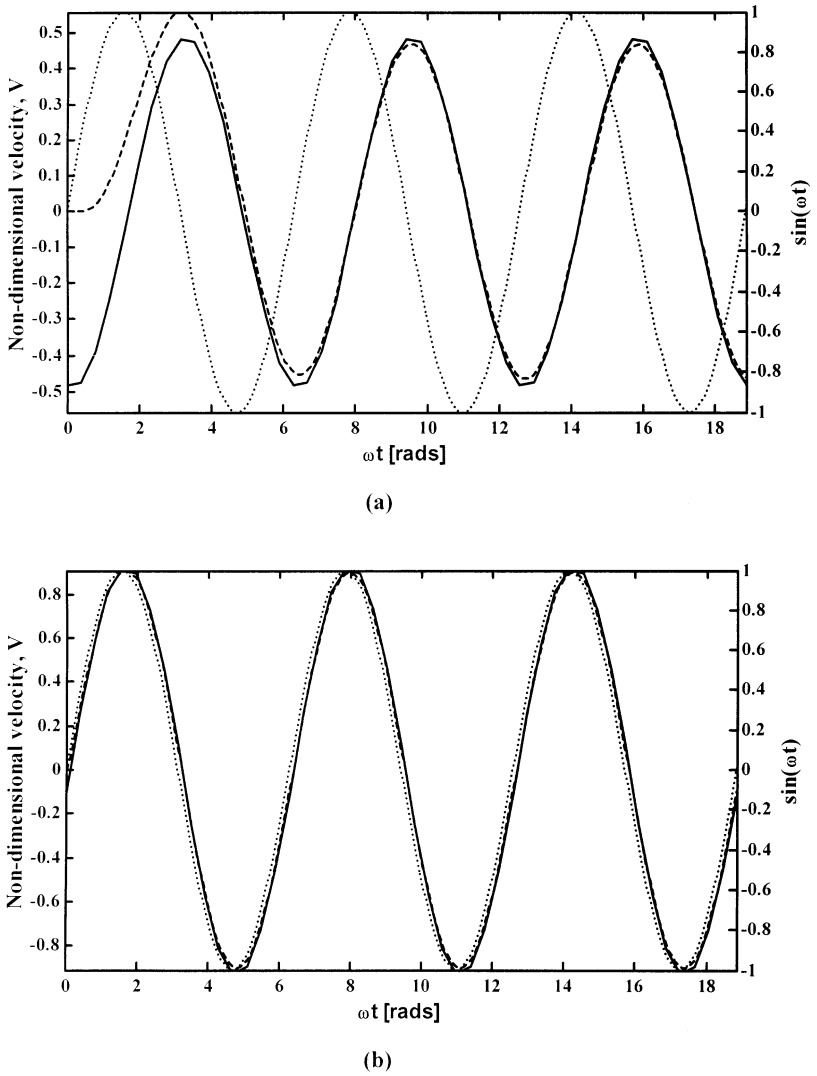

Figure 3. Transient and steady state time periodic velocity of (a) channel midpoint and (b) double-layer maxima at $\Omega = 30$. The dashed line represents the transient solution, eq 11, the solid line represents the steady state solution, eq 13, and the dotted line represents the scaled magnitude of the applied electric field.

corner (see above), deemed to be characteristic of the flow velocity in the double layer. Also shown in Figures 3 and 4 is the fully transient flow solution given by eq 11. From Figure 3, it is apparent that the response of the fluid within the double layer is nearly immediate; however, the bulk fluid lags behind the applied field by a phase shift of the order of $\pi/4$. Additionally, while the velocity in the double layer reaches its steady state oscillation almost immediately, the bulk flow requires just over a period before the transient effects are dissipated. In eq 13, the out-of-phase cosine term ($\Omega \cos(\Omega\theta)$) is proportionally scaled by Ω; thus as expected when Ω is increased in Figure 4, the phase shift for both the double-layer and bulk flow velocities is increased as is the number of cycles required to reach the steady state. Although the magnitude of the velocity at the channel midpoint is significantly decreased, to approximately 1% of that for the $\Omega = 30$ case, it is interesting to note the net positive velocity at the channel midpoint within the transient period before decaying into the steady state behavior. This is a result of the initial positive impulse given to the system when the electric field is first applied and is reflected by the exponential term in eq 11. The transient oscillations were observed to decay at an exponential rate, as expected from this transient term. Similar to the out-of-phase cosine term, this exponential term is also proportionally scaled by the nondimensional frequency, suggesting that the effect of the initial impulse becomes more significant with increasing Ω. Referring back to Figure 3a, this effect can also be observed at the peak of the first oscillation; the transient solution velocity (dashed line) is slightly higher than the time periodic (solid line) velocity. However, since Ω is much lower in this case the decay of this initial impulse is significantly faster.

III.A. Channel Aspect Ratio. While the square geometry is of significant theoretical interest, in most practical cases microchannels are significantly wider than deep (as a consequence of the micromachining technique), and thus it is of interest to examine the influence of the channel aspect ratio on the velocity profile. Figure 5 shows the time periodic velocity profile, from eq 13, in the upper right quadrant, at $t = \pi/\omega$ for an aspect ratio (width/depth) of 2:1 and 4:1 at the same oscillation frequencies as those shown in Figure 2. As can be seen within the corner region, the velocity profiles are very similar to those presented in Figure 2. However, at lower values of X (i.e., nearer the middle of the channel) the influence of the channel sidewall is reduced and the magnitude of the velocity is decreased, particularly prevalent in the low-frequency case. Extending this trend to the infinitely wide slit channel case where

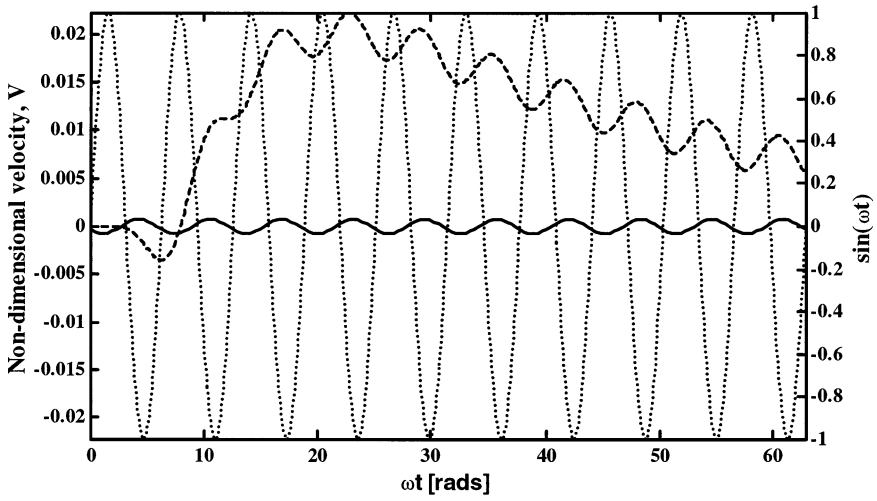

(a)

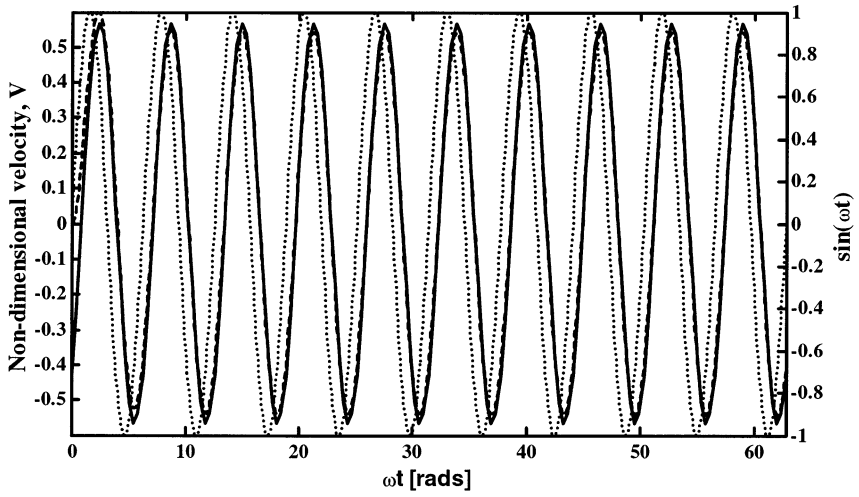

(b)

Figure 4. Transient and steady state velocity of (a) channel midpoint and (b) double-layer maxima at $\Omega = 625$. The dashed line represents the transient solution, eq 11, the solid line represents the steady state solution, eq 13, and the dotted line represents the scaled magnitude of the applied electric field.

$D_{h,slit} = 2D_{h,square}$ and thus $\Omega_{slit} = 4\Omega_{square}$, it can be concluded that the flow response in a slit channel will be comparable to that in an equivalent square channel at 4 times the applied frequency or with double the channel dimensions.

III.B. Influence of the Magnitude and Distribution of the ζ-Potential. As was outlined above, an inherent assumption in the analytical model (eq 11) is the double-layer field linearization via the Debye−Hückel approximation. This approximation is applicable to cases where $|\zeta| < 25$ mV and is somewhat restrictive since most practical applications of electroosmotic flow occur outside of this range. Thus it is desirable to examine both the influence of the ζ-potential on the flow field and the inherent error in the linearized model by comparing it with a numerical solution to the exact, nonlinear governing equations, eq 4 and eq 7. The full set of these equations was solved using the BLOCS (Bio-Lab-On-a-Chip Simulation) finite element simulation code (for details on the code and the numerical technique, the reader is referred to previous works[11,13,14,18]). The results of these numerical simulations are compared with the linearized solution, eq 11, along the $Y = 0$ edge in Figure 6 for (a) $\zeta = -25$ mV and (b) $\zeta = -100$ mV for both the $\Omega = 30$ and $\Omega = 625$ cases. By comparing these figures, it is apparent that increasing the ζ-potential increases the magnitude of the velocity, as expected; however, it has little effect on the flow structure, as both cases yield essentially identical velocity profiles. In each case, it is also apparent that the linearized analytical solution tends to slightly underestimate the actual flow velocity. An examination of the cause of this error revealed that the largest contributor was the $\sinh(\Psi) \approx \Psi$ approximation in the body force term of the Stokes equation, eq 8, whereas the error induced by the linear double-layer equation, eq 5, had a much smaller effect on the computed flow field. As can be seen, however, the magnitude of this error for all cases is less than 2%, suggesting that the linearized analytical solution is sufficiently accurate for most practical cases.

Many microfluidic channels have nonuniform surface properties either as a result of the fabrication process (for example microdevices fabricated in poly(dimethylsiloxane) (PDMS) devices are commonly bonded to a glass microscope slide to enclose the channel) or by heterogeneous

(18) Erickson, D.; Li, D. *Int. J. Heat Mass Transfer* **2002**, *45*, 3759.

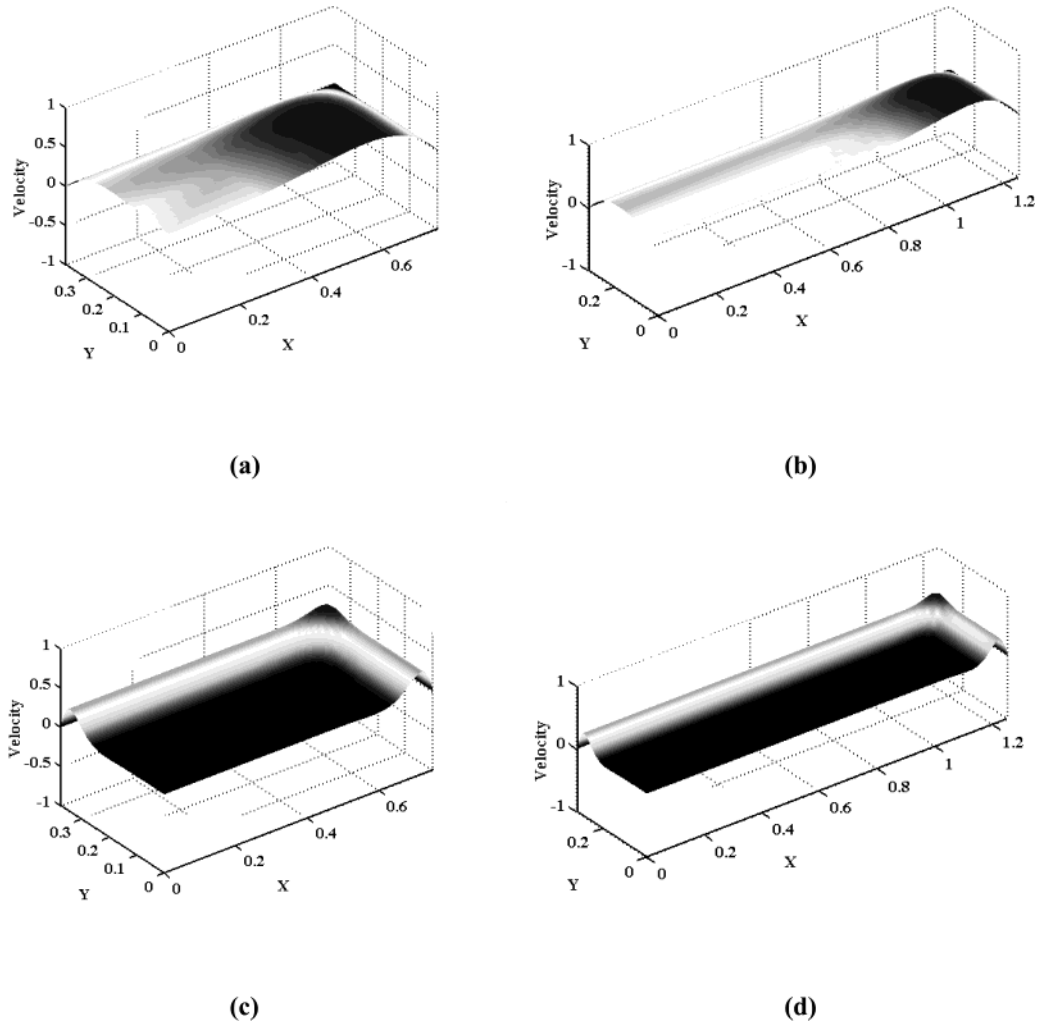

Figure 5. Steady state time periodic electroomostic velocity profiles at $t = \pi/\omega$ in a microchannel with (a) 2:1 aspect ratio and $\Omega = 30$, (b) 4:1 aspect ratio and $\Omega = 30$, (c) 2:1 aspect ratio and $\Omega = 625$, and (d) 4:1 aspect ratio and $\Omega = 625$.

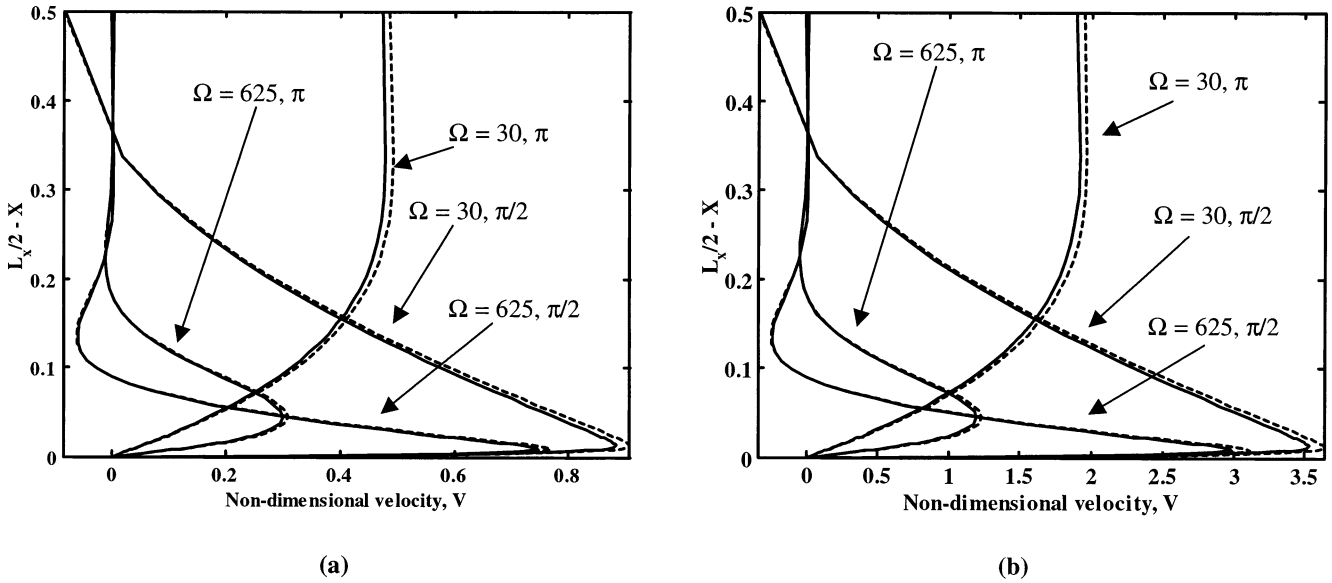

Figure 6. Steady state time periodic electroosmotic velocity profile along the $Y = 0$ edge for (a) $\zeta = -25$ mV and (b) $\zeta = -100$ mV. The dashed line represents the numerical solution to the nonlinear Poisson−Boltzmann distribution, and the solid line represents the Green's function solution.

adsorption of transported species/contaminants. It is of interest to examine how such a nonuniform ζ-potential distribution will affect the flow field. Figure 7 shows the time periodic velocity profiles at $t = \pi/2\omega$, as computed using the analytical solution, for the $\Omega = 30$ and $\Omega = 625$ cases with a neutral surface charge ($\zeta = 0$ mV) (a,b) and

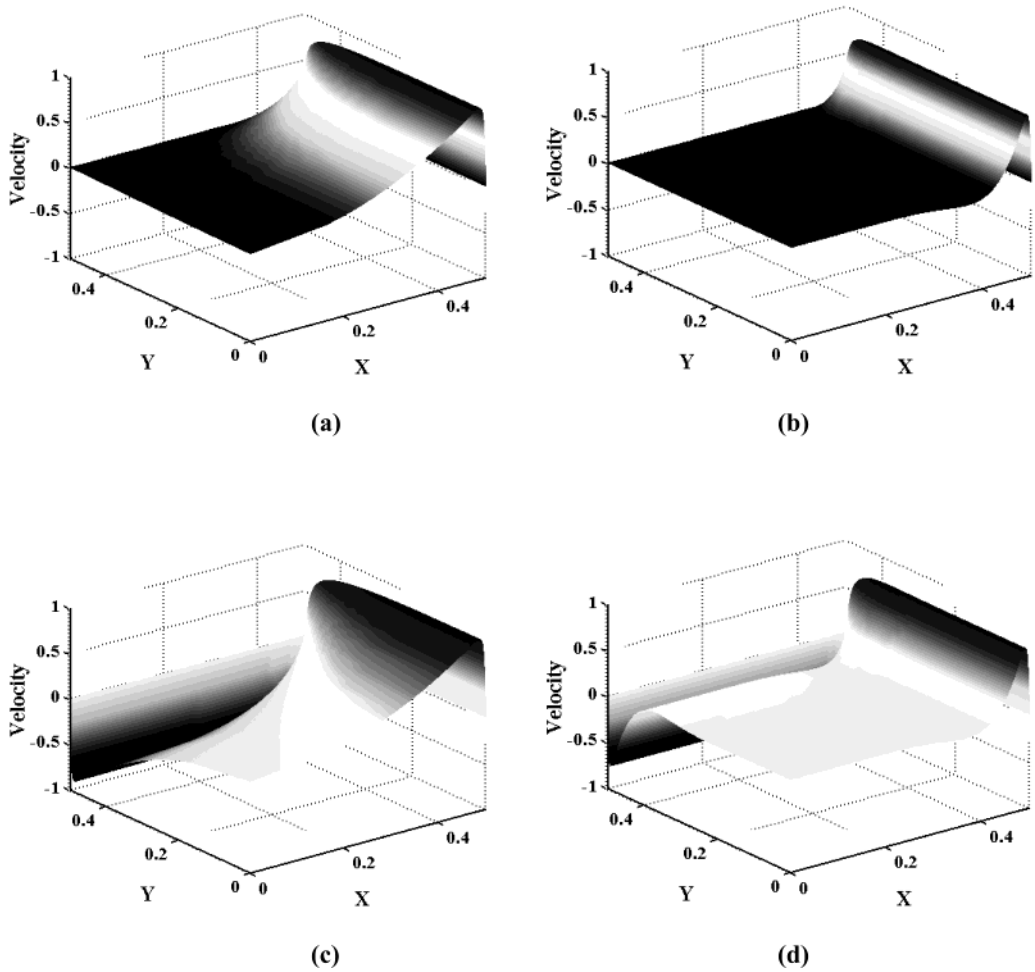

Figure 7. Steady state electroosmotic velocity profiles at $t = \pi/2\omega$ in a square microchannel with (a) $\zeta(Y = L_y/2) = 0$ mV and $\Omega = 30$, (b) $\zeta(Y = L_y/2) = 0$ mV and $\Omega = 625$, (c) $\zeta(Y = L_y/2) = +25$ mV and $\Omega = 30$, and (d) $\zeta(Y = L_y/2) = +25$ mV and $\Omega = 625$. In all cases $\zeta(X = L_x/2) = -25$ mV.

a positive surface charge ($\zeta = +25$ mV) (c,d) along the $Y = L_y/2$ surface, while the ζ-potential along the $X = L_x/2$ surface was maintained at $\zeta = -25$ mV. Along the neutral charged, $Y = L_y/2$, surface there is a zero net charge density in the nearby liquid (and thus no net body force applied to the fluid continua); the liquid remains stationary. This has a significant influence on the bulk flow field in the region near this surface, but the effect tended to diminish as the distance from this wall increased. Consequently, the maximum velocity occurs along the $Y = 0$ edge as opposed to the corner as was reported for the homogeneous case. Similarly, for the positive surface charge case the negative net charge density in the double layer induced a net flow opposite to that along the negatively charged surface, resulting in zero net volume flow rate at all times. For both cases, it is interesting to note that while the surface heterogeneity does significantly affect the bulk velocity profile, the velocity profile near the $X = L_x/2$ surface ($\zeta = -25$ mV) only exhibits a significant change in the corner region.

III.C. Examination of Different Excitation Waveforms. In the results presented above, we have limited our analysis to sinusoidal waveforms. As is described by Selvaganapathy et al.,[8] however, this may not be the ideal waveform for a particular application, and thus it is of interest to examine how the flow field will respond to different forms of periodic excitation, such as a square (step) or triangular waveform as defined by eq 14 and eq 15, respectively.

$$F(\Omega\theta) = \begin{Bmatrix} +1 & 2n\pi < \Omega\theta \le (2n+1)\pi & n = 0, 1, 2, 3 \ldots \\ -1 & (2n+1)\pi < \Omega\theta \le (2n+2)\pi & n = 0, 1, 2, 3 \ldots \end{Bmatrix} \quad (14)$$

$$F(\Omega\theta) = \begin{Bmatrix} 2(\Omega\theta - 2n\pi)/\pi & 2n\pi < \Omega\theta \le (4n+1)\pi/2 & n = 0, 1, 2, 3 \ldots \\ 2 - 2(\Omega\theta - 2n\pi)/\pi & (4n+1)\pi/2 < \Omega\theta \le (4n+3)\pi/2 & n = 0, 1, 2, 3 \ldots \\ 2(\Omega\theta - 2n\pi)/\pi - 4 & (4n+3)\pi/2 < \Omega\theta \le (2n+2)\pi & n = 0, 1, 2, 3 \ldots \end{Bmatrix} \quad (15)$$

Figure 8 compares the time periodic velocity profiles, along the $Y = 0$ axis, for the three waveforms (sin, square, and triangular) at (a) $\Omega = 31$ and (b) $\Omega = 625$ in a square channel by numerical solution to the exact, nonlinear governing equations, eq 4 and eq 7. As can be seen in all cases, the square waveform yields higher local velocities because the full strength of the electric field is applied for a longer time. It is apparent from these figures that the particular waveform has a greater affect on the flow field at lower Ω (i.e., at lower frequencies or smaller channel dimensions). A lower Ω corresponds to a smaller diffusion time scale in comparison with the excitation period, and thus the velocity in the bulk flow is more representative of the instantaneous magnitude of the applied field. Figure 9 shows that the particular waveform also has a significant effect on the transient response of the bulk fluid (again the channel midpoint is chosen as a representative point). As can be seen in Figure 9a for the $\Omega = 30$ case, and as was noted above, a square wave excitation tends to produce higher velocities whereas the triangular wave exhibits

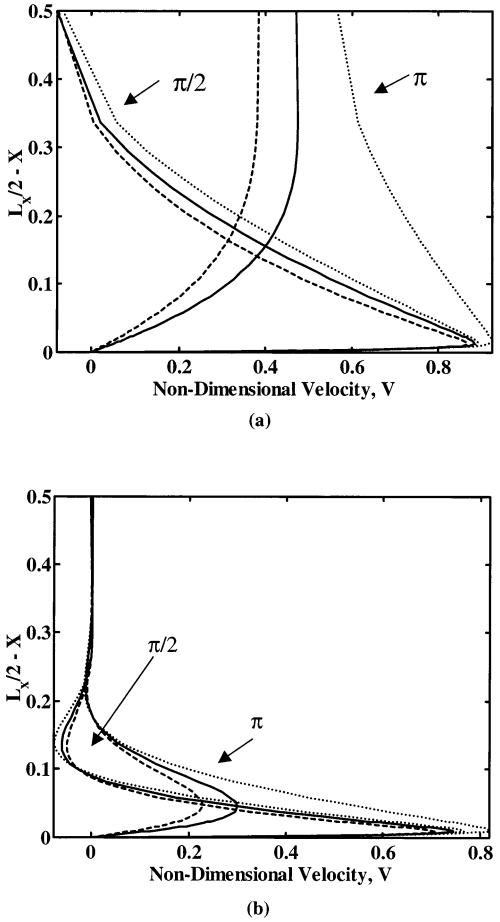

Figure 8. Steady state time periodic electroosmotic velocity profiles for different applied electric field waveforms along the $Y = 0$ edge for (a) $\Omega = 30$ and (b) $\Omega = 625$. The solid line represents the sin wave, the long-dashed line represents the triangular wave, and the dotted line represents the square wave.

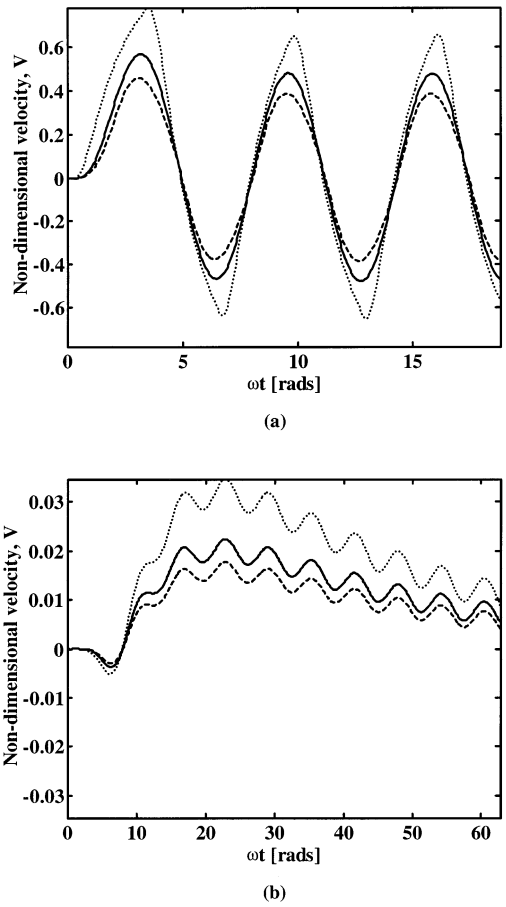

Figure 9. Transient stage velocity at channel midpoint for impulsively started flows using different waveforms at (a) $\Omega = 30$ and (b) $\Omega = 625$. The solid line represents the sin wave, the long-dashed line represents the triangular wave, and the dotted line represents the square wave.

slightly smaller bulk velocities when compared with the sinusoidal waveform. As Ω is increased, the initial positive impulsive velocity seen earlier in Figure 4a is again observed for both additional waveforms as shown in Figure 9b. As expected, the fluid excited by the square waveform exhibits higher instantaneous velocities, which lead to an increase in the number of cycles required to reach the steady state oscillation.

III.D. Brief Comments on the Practical Aspects. In the above work, we have mathematically and numerically described uniaxial electroosmotic flow field in a square microchannel subject to an oscillating electric field. As is mentioned in the Introduction, ac electroosmosis has a number of applications in microfluidic and microelectromechanical system (MEMS) devices.[1,4−10] The governing parameter in the above formulation is Ω which represents the ratio of the diffusion time scale ($t_{diff} = \rho_f D_h^2/\mu$) to the period of the applied electric field ($t_E = 1/\omega$). Table 1 shows the frequencies required to obtain the flow patterns described in this work (i.e., $\Omega = 30$ and $\Omega = 625$) for channel sizes typically found in microfluidic devices. These frequencies cover the range that has been applied to microfluidic devices, from the relatively low frequencies used by Oddy et al.[1] (5−20 Hz) to the high frequencies used by Green et al.[4] (as high as 1 MHz).

Table 1. Applied Frequency to Obtain the Described Flow Fields for Typical Microfluidic Channel Sizes

$\Omega = \rho_f D_h^2 \omega/\mu$	channel hydraulic diameter $D_h = 4l_x l_y/2(l_x + l_y)$ (μm)	frequency
30	10	48 kHz
	50	1.9 kHz
	200	120 Hz
	300	50 Hz
625	10	1 MHz
	50	40 kHz
	200	2.5 kHz
	300	1.1 kHz

IV. Conclusions

In this study, a Green's function solution to the time periodic flow in a rectangular microchannel with non-uniform ζ-potential is presented for the special case of an applied sinusoidal electric field. The flow response to excitation by more complex waveforms is also investigated using the BLOCS finite element code.

In general, it is shown that the time periodic velocity profile is governed by a nondimensional parameter $\Omega = \rho_f D_h^2 \omega/\mu$ which defines the ratio of the time scale for viscous diffusion to the period of oscillation. In cases of high Ω (i.e., high excitation frequency or large channel sizes), the flow is shown to be confined to a region near the channel wall while the bulk fluid remains essentially stationary. Both the channel's ζ-potential distribution and aspect ratio are shown to have a significant effect on the velocity profile. In uniform channels, however, the ζ-potential serves only to scale the magnitude of the velocity and does not significantly affect the flow structure. Impulsively started flows (from rest) are also shown to exhibit transient

behavior resulting in a net positive flow during the initial cycles for cases of high Ω. Additionally, the number of cycles required reaching a steady state oscillation increases with Ω. At higher Ω, the excitation waveform (sinusoidal, square, or triangular) has little effect on the velocity profile. However, as Ω approaches unity, viscous diffusion is sufficiently fast to allow the bulk flow to respond to instantaneous changes in the applied electric field, and the influence of a particular waveform is shown to be more significant.

Acknowledgment. The authors are thankful for the financial support of the Natural Sciences and Engineering Research Council through a scholarship to David Erickson and through a research grant to D. Li.

LA027035S